International Journal of Research
Available at https://edupediapublications.org/journals
p-ISSN: 2348-6848
e-ISSN: 2348-795X
Volume 03 Issue 14
October 2016

Ear Identification System Based On Multi-Model Approach

Dheyaa abbood chyad
Master's in Computer Science
University of Basrah

Dr. Abbas H. Hassin Alasadi
Assistant Professor
University of Basrah

Abstract:

The propose of the study is to ear Identification system in view of 2D ear images which incorporates in three phases: they are ear enrollment, ear extraction, ear Identification and confirmation. Ear enlistment incorporates ear detection and ear normalization. The ear identification approach in light of enhanced skin location technique identifies the ear part under complex foundation utilizing calculation Ycbcr. At that point Morphological close picture is connected to portion the ear part and standardize all the ear pictures to a similar size and ear extraction. Euclidean separation measure (EDM) is then connected for measurement decrease of the high-dimensional Gabor highlights. At last separation based classifier is connected for ear acknowledgment. Trial aftereffects of ear acknowledgment on sub-datasets and the execution of the ear ID framework demonstrate the attainability and viability of the proposed approach.

Keywords: Ear Identification and Verification, Euclidean distance measure (EDM), Morphological close image, Scale-invariant feature transform, Skin Detection (Ycbcr).

INTRODUCTION:

The research on ear recognition has been drawing increasingly consideration in late five years. In view of the exploration of the "Iannarelli system", the structure of the ear is

genuinely steady and vigorous to changes in outward appearances or maturing. Ear biometrics is noncontacting thus it can be connected for human distinguishing proof at a separation, making it an accommodating supplement to facial recognition. An ear recognition system in light of 2D pictures is made out of the accompanying stages: ear enlistment, highlight extraction, and ear recognition/authentication. The phase of ear enlistment incorporates programmed ear detection and ear standardization. Ear detection concentrates on distinguishing human ear from the info pictures and after that finding and portioning every ear in the picture. At that point all the ear pictures are standardized to a similar size in light of some predefined standard. Next stride is to speak to the ear by proper elements, for example, basic elements, neighborhood highlights, and all encompassing elements. At last viable classifier will be intended for ear recognition or authentication, for example, closest neighbor classifier, inadequate representation classifier, RBF classifier, or SVM classifier [1].

The present study concentrate for the most part centered around highlight extraction and grouping. The ear images are for the most part physically separated for later handling. The arrangement procedure was not obviously outlined in a large portion of the ear recognition papers. So the ear pictures utilized as a part of various strategies were not standardized in light of a similar standard. In this way the examinations among various strategies are less important. So [6, 7] proposed programmed ear detection in light of Adaboost calculation. The ear parts exhibited in source pictures are divided. Be that as it may, these fragmented ear pictures may contain the "unadulterated

ear," as well as some foundation picture, (for example, confront profile and hair). This implies notwithstanding for a similar subject, the extent of each "immaculate ear" on the enlisted pictures in the dataset might be distinctive, and it is additionally conceivable that the measure of ears on the enrolled pictures is not the same as that of the ear to be verified. Such a large number of appearance based techniques won't work in this circumstance. This implies there exists a hole between ear detection and highlight extraction. This hole is programmed ear standardization, particularly like face normalization, which implies that we need to set up a standard to standardize the ear into a similar size. In this paper, we consolidate ear detection and ear standardization into one phase named ear enlistment. To our best learning, the exploration on ear enlistment is still an open zone [2].

RELATED WORK:

According to Phung, S. L., Bouzerdoum, A., & Chai, D. (2002), paper presents a new human skin color model in YCbCr color space and its application to human face detection. Skin colours are displayed by an arrangement of three Gaussian clusters, each of which is described by a centroid and a covariance grid. The centroids and covariance grids are assessed from substantial arrangement of preparing tests after a k-implies bunching process. Pixels in a shading input picture can be ordered into skin or non-skin in light of the Mahalanobis separations to the three clusters. Proficient post-preparing procedures to be specific clamor expulsion, shape criteria, elliptic bend fitting and face/non-confront characterization are proposed keeping in mind the end goal to assist refine skin division comes about with the end goal of face detection.

According to Kekre, H. B., & Thepade, S. D. (2009), Block Truncation Coding (BTC) based features is one of the CBIR methods proposed using color features of image. The approach fundamentally considers red, green and blue planes of picture together to register include vector. Here we have supported this BTC based CBIR as BTC-YCbCr and Spatial BTC-YCbCr. Here YCbCr shading space is considered. In BTC-YCbCr highlight vector is figured by considering Y, Cb and Cr planes of the picture autonomously. While in Spatial BTC-YCbCr , the element vector is made out of four sections. Every part is speaking to the elements removed from one of the four non covering quadrants of the picture. The new proposed strategies are tried on the database of 1000 pictures and the outcomes demonstrate that the exactness is enhanced in Spatial BTC-YCbCr and review is better in BTC-YCbCr. On the off chance that both accuracy and review are viewed as together Spatial BTC-YCbCr beats alternate strategies talked about in the paper.

According to Lin, C. (2007), investigation develops an efficient face detection scheme that can detect multiple faces in color images with complex environments and different illumination levels. The proposed scheme comprises two stages.The main stage embraces shading and triangle-based division to hunt potential face areas. The second stage includes confront check utilizing a multilayer feedforward neural system. The system can deal with different sizes of confronts, distinctive brightening conditions, various stance and alterable expression. Specifically, the plan fundamentally expands the execution speed of the face detection calculation on account of complex foundations. Aftereffects of this study show that the

proposed technique performs superior to anything past strategies as far as speed and capacity to handle diverse brightening conditions.

METHODOLOGY:

YCrCb color space:

Many researchers have proposed various techniques to detect human faces from images. In YCrCb color space was used to detect faces in the context of video sequences. A two-dimensional Cr-Cb histogram was employed for separating a facial region from the back-ground and a region-growing technique was applied on the remaining area. Finally faces are detected by ellipse matching and using criteria based on face's characteristics under a normal illumination condition, the skin color falls into a small region on the CbCr plane, and the luminance (Y) is uncorrelated with respect to the CbCr. Thus, a pixel is classified as skin-like if its chrominance value falls into the small region defined in CbCr plane, and the luminance (Y) falls into the interval defined empirically. Many different methods for discriminating between skin and non-skin pixels are available in the literature. These can be gathered in three sorts of skin displaying: parametric, nonparametric, and express skin bunch definition techniques. The Gaussian parametric models accept that skin shading circulation can be displayed by a circular Gaussian joint likelihood thickness work. Nonparametric techniques gauge skin shading dispersion from the histogram of the preparation information without determining an express model of skin shading model [3].

The YCbCr shading space is broadly utilized for advanced picture. In this configuration, luminance data is put away as a solitary segment (Y), and chrominance data is put away as two

shading contrast segments (Cb and Cr). Cb speaks to the contrast between the blue segment and a reference esteem. Cr speaks to the contrast between the red segment and a reference esteem. YCbCr information can be twofold exactness, yet the shading space is especially appropriate to uint8 information. For uint8 pictures, the information run for Y and the range for Cb and Cr. YCbCr

- RGB = imread('flowers.tif');
- YCBCR = rgb2ycbcr(RGB);

Figure 1: Block Diagram of YCbCr Model

EAR IDENTIFICATION & EXTRACTION:

Closing is an important operator from the field of mathematical morphology. Like its dual operator opening, it can be derived from the fundamental operations of erosion and dilation. Like those operators it is normally applied to binary images, although there are graylevel versions. Closing is similar in some ways to dilation in that it tends to

leaves room at the top and base of the full uint8 territory so that extra (non-picture) data can be incorporated into a video stream. The capacity rgb2ycbcr changes over shading maps or RGB pictures to the YCbCr shading space. ycbcr2rgb plays out the turn around operation. For instance, these orders change over the blooms picture to YCbCr arrange.

enlarge the boundaries of foreground (bright) regions in an image (and shrink background color holes in such regions), but it is less destructive of the original boundary shape. As with other morphological operators, the exact operation is determined by a structuring element. The effect of the operator is to preserve background regions that have a similar shape to this structuring element, or that can completely contain the structuring element, while eliminating

all other regions of background pixels [4].

As with erosion and dilation, this particular 3×3 structuring element is the most commonly used, and in fact many implementations will have it hardwired into their code, in which case it is obviously not necessary to specify a separate structuring element. To achieve the effect of a closing with a larger structuring element, it is possible to perform multiple dilations followed by the same number of erosions. Closing can sometimes be used to selectively fill in particular background regions of an image. Whether or not this can be done depends upon whether a suitable structuring element can be found that fits well inside regions that are to be preserved, but doesn't fit inside regions that are to be removed [5].

A * B = (A B) B

Where ⊕ and ⊖ denote the dilation and erosion, respectively. In imageprocessing,losing is, together with opening, the basic workhorse of morphological noise removal. Opening removes small objects, while closing removes small holes [6].

Scale Invariant Feature Transforms

For any object there are many features, interesting points on the object that can be extracted to provide a "feature" description of the object. This description can then be used when attempting to locate the object in an image containing many other objects. There are many considerations when extracting these features and how to record them. SIFT image features provide a set of features of an object that are not affected by many of the complications experienced in other methods, such as object scaling and rotation. While allowing for an object to be recognised in a larger image SIFT

image features also allow for objects in multiple images of the same location, taken from different positions within the environment, to be recognised. SIFT features are also very resilient to the effects of "noise" in the image. The SIFT approach, for image feature generation, takes an image and transforms it into a "large collection of local feature vectors". Each of these feature vectors is invariant to any scaling, rotation or translation of the image [7].

This stage of the filtering attempts to identify those locations and scales that are identifiable from different views of the same object. This can be efficiently achieved using a "scale space" function. Further it has been shown under reasonable assumptions it must be based on the Gaussian function. The scale space is defined by the function:

$$L(x, y, \sigma) = G(x, y, \sigma) * I(x, y)$$

Where * is the convolution operator, $G(x, y, \sigma)$ is a variable-scale Gaussian and $I(x, y)$ is the input image. Various techniques can then be used to detect stable keypoint locations in the scale-space. Difference of Gaussians is one such technique, locating scale-space extrema, $D(x, y, \sigma)$ by computing the difference between two images, one with scale k times the other. $D(x, y, \sigma)$ is then given by [8]:

$$D(x, y, \sigma) = L(x, y, k\sigma) - L(x, y, \sigma)$$

To detect the local maxima and minima of $D(x, y, \sigma)$ each point is compared with its 8 neighbours at the same scale, and its 9 neighbours up and down one scale. If this value is the minimum or maximum of all these points then this point is an extrema.

From the image above, it is obvious that we can't use the same window to detect keypoints with different scale. It is OK with small

corner. But to detect larger corners we need larger windows. For this, scale-space filtering is used. In it, Laplacian of Gaussian is found for the image with various σ values. LoG acts as a blob detector which detects blobs in various sizes due to change in σ. In short, σacts as a scaling parameter. For eg, in the above image, gaussian kernel with low σgives high value for small corner while guassian kernel with high σfits well for larger corner. So, we can find the local maxima across the scale and space which gives us a list of (x, y, σ)values which means there is a potential keypoint at (x,y) at σscale. But this LoG is a little costly, so SIFT algorithm uses Difference of Gaussians which is an approximation of LoG. Difference of Gaussian is obtained as the difference of Gaussian blurring of an image with two different σ, let it be $\sigma$and $k\sigma$ [9].

A central problem in image recognition and computer vision is determining the distance between images. Considerable efforts have been made to define image distances that provide intuitively reasonable results. Among others, two representative measures are the tangent distance and the generalized Hausdorff distance. Tangent distance is locally invariant with respect to some chosen transformations, and has been widely used in handwritten digit recognition. The generalized Hausdorff distance is not only robust to noise but also allows portions of one image to be compared with another, and has become a standard tool for comparing shapes [10].

Among all the image metrics, Euclidean distance is the most commonly used due to its simplicity. Let x, y be two M by N images, $x = (x^1, x^2, \ldots, x^{MN})$, $y = (y^1, y^2, \ldots, y^{MN})$,

Euclidean Distance Measure

Where x^{kN+l}, y^{kN+l} are the gray levels at location (k,l) . The Euclidean distance (,) $E\ d\ x\ y$ is given by

A reasonable image metric should present smaller distance between (a), (b) than that of (a), (c). But the Euclidean distance gives counter intuitive result. For simplicity, let the gray levels be one at the black pixels and zero elsewhere. Computing the Euclidean distances yields (a, b) = 54 and (a, c) = 49. The pair with more similarity has a larger Euclidean distance! This phenomenon is caused by the fact that the Euclidean distance defined in (1) does not take into account that x, y are images, x^k , y^k are gray levels on pixels. For images, there are spatial relationships between pixels. The traditional Euclidean distance is only a summation of the pixel-wise intensity differences, and consequently small deformation may result in a large Euclidean distance. This paper proposes a new Euclidean distance, which we call Image Euclidean Distance (IMED). Unlike the traditional one, IMED takes into consideration the spatial relationships of pixels. Based on three properties that (arguably) any intuitively reasonable image metric should satisfy, we show that IMED is the only Euclidean distance possessing these properties. IMED is then applied to image recognition.

All the M by N images are easily discussed in an MN dimensional Euclidean space, called image space. It is natural to adopt the base e_1,e_2 ,…..,e_{MN} to form a coordinate system of the image space, where e_{KN+1} corresponds to an ideal point source with unit intensity at location $(k,_l)$. Thus an image $x = (x^1, x^2 ,……., x^{MN})$, where x^{kN+l} is the gray level at the (k, l)th pixel, is represented as a point in the image space, and x^{kN+l} is the coordinate with respect to e_{KN+1}. The origin of the image space is an image whose gray levels are

zero everywhere. Although the algebra of the image space can be easily formulated as above, the Euclidean distance of images could not be determined until the metric coefficients of the basis are given [11].

The metric coefficients $g_{i,j}$ i, j =1,2,……,MN , are defined as

$$g_{ij} = < e_i, e_j > = \sqrt{< e_i, e_i >} \sqrt{< e_j, e_j >} \cdot$$

where <,> is the scalar product, and $\theta_{i,j}$ is the angle between e_i and e_j. Note that, if $<e_i, e_j> = < e_i, e_j>$=…., all the base vectors have the same length, then ij g depends completely on the angle θ_{ij} . Given the metric coefficients, the Euclidean distance of two images x, y is written by

$$d_E^2(x,y) = \sum_{i,j=1}^{MN} g_{ij}(x^i - y^i)(x^j - y^j) = ($$

where the symmetric matrix will be referred to as metric matrix. For images of fixed size *M* by *N*, every *MN* th order symmetric and positive definite matrix *G* induces a Euclidean distance. But most of them are not appropriate for measuring image distances. For example, suppose any two base vectors $e_i, e_j (i \neq j)$, no matter which pixels they correspond to, are mutually perpendicular, the basis then forms a Cartesian coordinate system. Accordingly, *G* is the identity matrix, and it induces the traditional Euclidean distance given by (1). (If the base vectors have different lengths, *G* is a diagonal matrix. It induces the weighted Euclidean distance.) We have illustrated in the previous section this traditional metric's sensitivity to deformation, which is caused by the regardless of the fact that the two objects being compared are images. Geometrically, this defect is due to the orthogonality of the base vectors $e_1, e_2, \ldots, e_{MN}$, which correspond to pixels.

The reader should be aware that two distances are being discussed here, one is the image distance measured in the

high dimensional image space, the other is the pixel distance. Let P_i, P_j, i, j = 1, 2 be pixels. The pixel distance, written as $|P_i - P_j|$, is the distance between $P_i$and $P_j$on the image lattice. For example, if $P_i$is at location (k, l), and $P_j$is at (k',l') , $|P_i - P_j|$may be . Consider a simplification of the images (a), (b). Let the two digits seven, denoted by *x*, *y* respectively, are different on only two pixels $P_i$and P_j. Their Euclidean distance is completely determined by $g_{i,j}$, or $\theta_{i,j}$if $g_{ii}= g_{jj}= 1$, i.e. $e_i$and $e_j$have the unit length. It is a small deformation because $P_i$and $P_j$are close to each other. In the traditional Euclidean distance, we set $\theta_{i,j} =\pi/2$. Then $g_{ij} = \cos\theta_{ij}= 0$, hence

$$d_E(x,y)=\sqrt{g_{ii}(x^i-y^i)^2+g_{jj}(x^j-y^j)^2+2g_{ij}(x^i-y^i)(x^j-y^j)}=\sqrt{g_{ii}+g_{jj}}=\sqrt{2}.$$

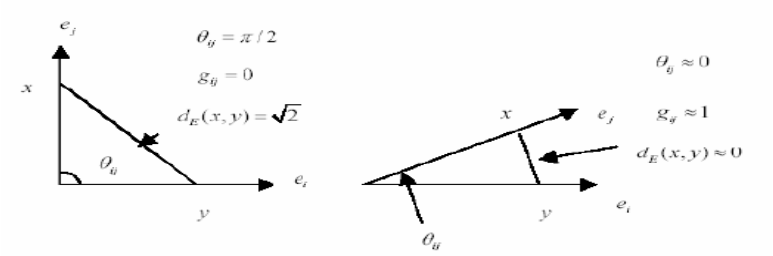

Figure 2: Depending properly on pixel distance, metric coefficients induce a Euclidean distance that is robust to small deformation.

There exist fast algorithms for ST, i.e. $u = G^{1/2}x = \Gamma \Lambda^{1/2} \Gamma^T x$. Note that *G* is separable

$$g_{iN+j,i'N+j'}=\exp\left\{-\left[(i-i')^2+(j-j')^2\right]/2\right\}=\exp\left\{-(i-i')^2/2\right\}\cdot\exp\left\{-(j-j')^2/2\right\}$$

The *MN* by *MN* matrix *G* can be written as the Kronecker product of an *M* by *M* and an *N* by *N* matrices. Consequently, the eigenvectors of *G* , i.e. Γ , is also separable. The transformation $\Gamma^T x$ can be realized by a succession of two one-dimensional transforms on *x*. Moreover, most entries of $G^{1/2}$ are nearly zero, so ST may be well approximated in spatial domain by a 5×5 mask for a practical

use [12]. Finally, we pointed out that IMED must NOT be understood as a Mahalanobis distance given by

$$d_M^2(\xi,\eta) = (\xi-\eta)^T \Sigma^{-1}(\xi-\eta)$$

That is, the matrix G in IMED (see (3)) must NOT be viewed as some inverse covariance matrix Σ^{-1}, although both G and Σ^{-1} are symmetric and positive definite matrices. On the surface, IMED and Mahalanobis distance have similar expressions. However, the two distance measures are essentially different for the following two reasons: 1) In the derivation of IMED, no random variables or statistics were involved. 2) More importantly, the Mahalanobis distance has a completely opposite behavior to IMED. That is, Mahalanobis distance is even more sensitive to small deformation than the traditional Euclidean distance. In fact, the covariance matrix Σ of images (random fields) have been studied in KLT based image compression for a long time. One of the commonly used covariance model $\Sigma = (\sigma_{ij})_{MNxMN}$ is given by

Comparing it to it is Σ but not $\Sigma-1$ that is similar to G. Accordingly, using this Mahalanobis distance for image recognition leads to an opposite effect to IMED.

RESULTS

The study results shows that the efficient working of ear identification and verification system. The results under go three stages of operations: Ear Extraction using Skin detection by YCBCR color space algorithm, Ear Detection using Morphological Closing image, Ear Identification and verification using SIFT (Scale-invariant feature transform) and EDM (Euclidean Distance Measure) [13].

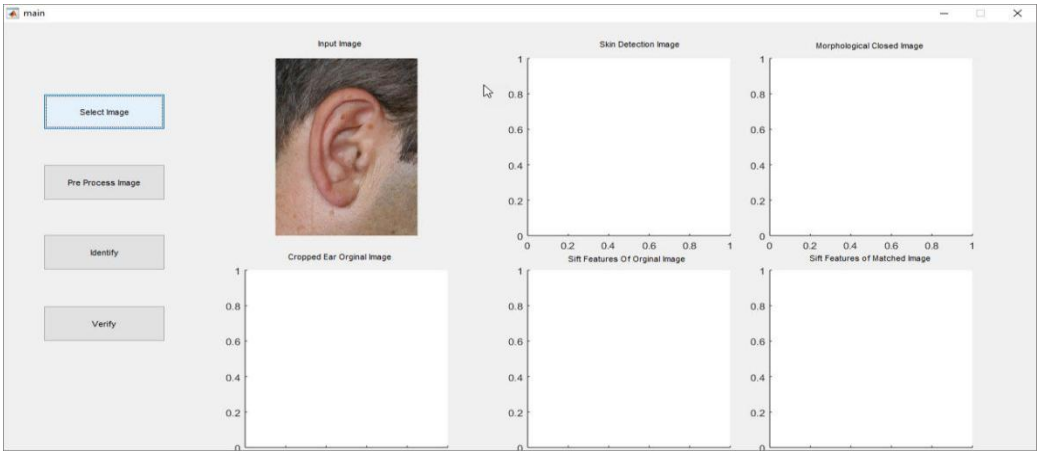

Figure 3: Ear input

In the first stage of process the system takes a ear image as input image and under goes process.

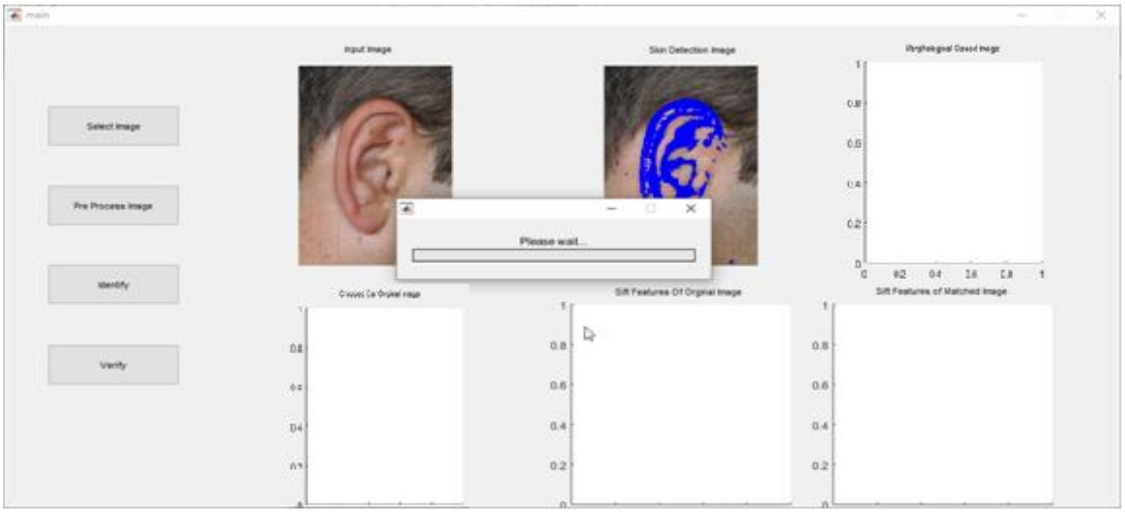

Figure 4: Ear extraction using skin detection

The second stage of the process is identification of ear from the input image using skin detection system by Ycbcr color space. The method analysis the The definitions of the R', G', and B' signals also differ between BT.709 and BT.601, and differ within BT.601 depending on the type of TV system in use (625-line as in PAL and SECAM or 525-line as in NTSC), and differ further in other specifications. In different designs there are differences in the

definitions of the R, G, and B chromaticity coordinates, the reference white point, the supported gamut range, the exact gamma pre-compensation functions for deriving R', G' and B' from R, G, and B, and in the scaling and offsets to be applied during conversion from R'G'B' to Y′CbCr. So proper conversion of Y′CbCr from one form to the other is not just a matter of inverting one matrix and applying the other. In fact, when Y′CbCr is designed ideally, the values of K_B and K_R are derived from the precise specification of the RGB color primary signals, so that the luma (Y′) signal corresponds as closely as possible to a gamma-adjusted measurement of luminance (typically based on the CIE 1931 measurements of the response of the human visual system to color stimuli).

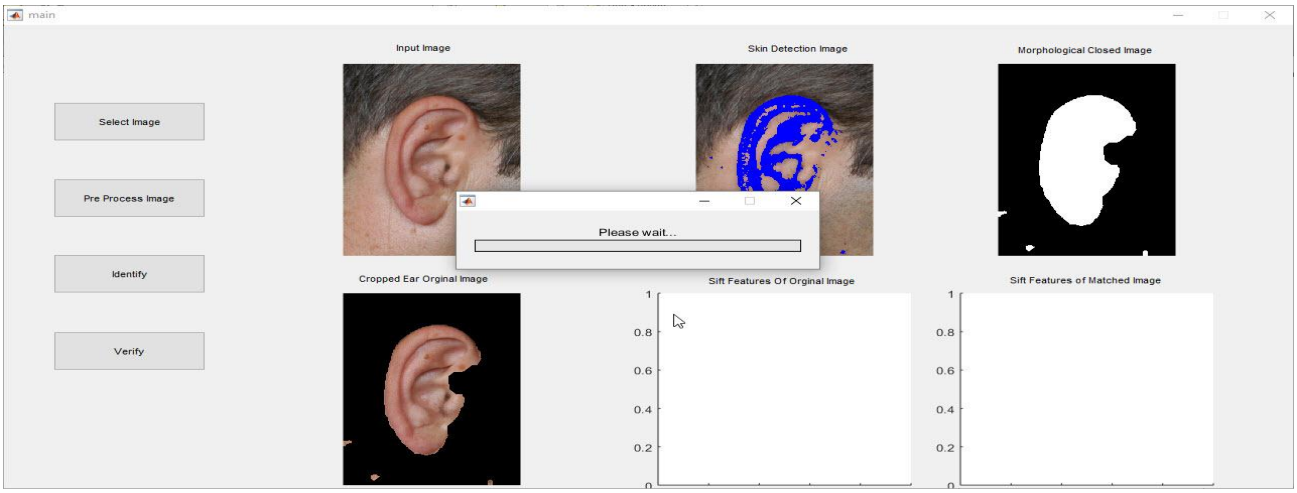

Figure 5: Ear Extraction using morphological close image

In the third procedure the ear extraction is done utilizing morphological close picture handling strategy. Where by the playing out a disintegration on the picture after the expansion, i.e. an end, we lessen some of this impact. The impact of shutting can be effectively imagined. Envision taking the organizing component and sliding it around outside every frontal area locale,

without changing its introduction. For any foundation limit point, if the organizing component can be made to touch that point, with no part of the component being inside a frontal area district, then that point remains foundation. In the event that this is impractical, then the pixel is set to closer view.M2 = imclose(IM,SE) performs morphological closing on the grayscale or binary image IM, returning the closed image, IM2. The structuring element, SE, must be a single structuring element object, as opposed to an array of objects. The morphological close operation is a dilation followed by erosion, using the same structuring element for both operations. IM2 = imclose(IM,NHOOD) performs closing with the structuring element strel(NHOOD), where NHOOD is an array of 0's and 1's that specifies the structuring element neighborhood. gpuarrayIM2 = imclose(gpuarraryIM,___) performs the operation on a graphics processing unit (GPU), where gpuarrayIM is a gpuArray containing the grayscale or binary image. gpuarrayIM2 is a gpuArray of the same class as the input image.

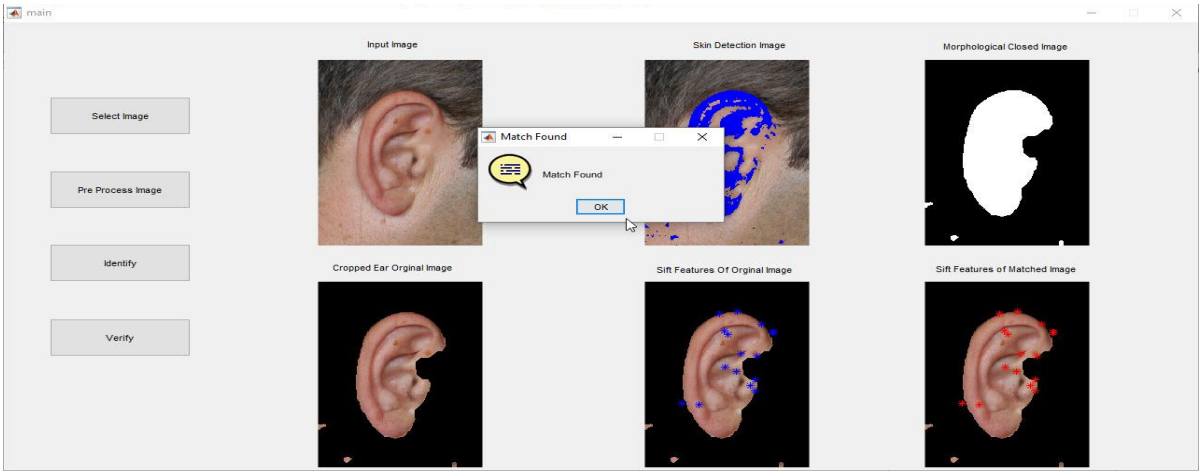

Figure 6: Ear Identification

In the fourth stage, after the ear identification process we move to ear identification process. Here the image is identified by matching the input image using SIFT and EDM method. SIFT keypoints of objects are first extracted from a set of reference images and stored in a database. A object is perceived in a new image by exclusively contrasting every element from the new image to this database and discovering applicant coordinating elements in light of Euclidean separation of their element vectors. From the full arrangement of matches, subsets of keypoints that concur on the question and its area, scale, and introduction in the new picture are distinguished to sift through great matches. The assurance of predictable clusters is performed quickly by utilizing a productive hash table usage of the summed up Hough change. Every bunch of at least 3 includes that concur on a protest and its posture is then subject to assist point by point display confirmation and in this manner exceptions are disposed of. At last the likelihood that a specific arrangement of components demonstrates the nearness of a question is registered, given the precision of fit and number of plausible false matches. This is a quick strategy for giving back the closest neighbor with high likelihood, and can give speedup by element of 1000 while finding closest neighbor (of intrigue) 95% of the time.

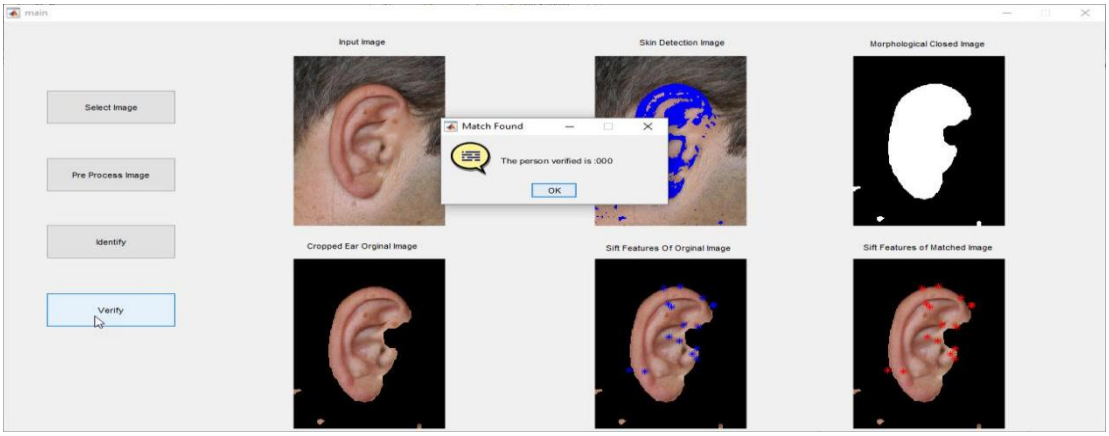

Figure 7: Ear Verification

By using the above explained SIFT and EDM the image verification process is carried in Matlab [14].

CONCLUSION

In this paper, an ear Identification System based on images is proposed. The primary commitments of the proposed strategy are the accompanying: (1) Ear Extraction utilizing Skin detection by YCBCR shading space calculation, Ear Detection utilizing Morphological Closing picture, Ear Identification and confirmation utilizing SIFT (Scale-invariant component change) and EDM (Euclidean Distance Measure). Examination. Trial comes about demonstrate that we can accomplish programmed ear recognition in light of 2D pictures with the proposed technique. Our future work will be centered around two viewpoints: (1) in the ear standardization arrange, we have to enhance the exactness of the ear cartilage limitation, create ponder models for the ear cartilage historic points, and make the seeking procedure less subject to the underlying model shape, and (2) in the ear authentication organize, we require a bigger dataset to affirm the coordinating precision and the continuous execution of the proposed strategy.

REFERENCE

1. R.Bajcsy, and S. Lovacic, "Multiresolution Elastic Matching," Computer Vision, Graphics, and Image Processing, vol. 46, pp. 1-21, 1989.
2. S. Bochner, Lectures on Fourier Integrals, Translated by M. Tenenbaum, and H. Pollard, Princeton University Press, Princeton, New Jersey, 1959.
3. J. Canny, "A Computational Approach to Edge Detection," IEEE Trans. Pattern Analysis and Machine Intelligence, vol. 8, no. 6, pp. 679-698, 1986.
4. D.P. Huttenlocher, G.A. Klanderman, and W.J. Rucklidge,

"Comparing Images Using the Hausdorff Distance," IEEE Trans. Pattern Analysis and Machine Intelligence, vol. 15, no. 9, pp. 850-863, Sep. 1993.

5. Wolfram, A., Fussel, D., Brune, T., & Isermann, R. (2001). Component-based multi- odel approach for fault detection and diagnosis of a centrifugal pump. In American Control Conference, 2001. Proceedings of the 2001 (Vol. 6, pp. 4443-4448). IEEE.
6. Boukhris, A., Mourot, G., & Ragot, J. (1999). Non-linear dynamic system identification: a multi-model approach. International Journal of Control, 72(7-8), 591-604.
7. Lu, L., Zhang, X., Zhao, Y., & Jia, Y. (2006, August). Ear recognition based on statistical shape model. In First International Conference on Innovative Computing, Information and Control-Volume I (ICICIC'06) (Vol. 3, pp. 353-356). IEEE.
8. Mazinan, A. H., & Sadati, N. (2010). Fuzzy predictive control based multiple models strategy for a tubular heat exchanger system. Applied Intelligence, 33(3), 247-263.
9. Cen, Z., Wei, J., & Jiang, R. (2013). A gray-box neural network-based model identification and fault estimation scheme for nonlinear dynamic systems. International journal of neural systems, 23(06), 1350025.
10. Schulte, H., & Hahn, H. (2001). Identification with blended multi-model approach in the frequency domain: an application to a servo pneumatic actuator. In *Advanced Intelligent Mechatronics, 2001. Proceedings. 2001 IEEE/ASME International Conference on* (Vol. 2, pp. 757-762). IEEE.

11. Yan, P., & Bowyer, K. W. (2006, June). An Automatic 3D Ear Recognition System. In *3DPVT* (pp. 326-333).
12. Aibinu, A. M., Salami, M. J. E., Shafie, A. A., Hazali, N., & Termidzi, N. (2011, January). Automatic fruits identification system using hybrid technique. In *Electronic Design, Test and Application (DELTA), 2011 Sixth IEEE International Symposium on* (pp. 217-221). IEEE.
13. Yan, P. (2006). *Ear biometrics in human identification* (Doctoral dissertation, University of Notre Dame).
14. Charfi, N., Trichili, H., Alimi, A. M., & Solaiman, B. (2016). Bimodal biometric system for hand shape and palmprint recognition based on SIFT sparse representation. *Multimedia Tools and Applications*, 1-26.